Available online at www.sciencedirect.com
ScienceDirect
Journal of Solid State Chemistry 181 (2008) 508–514
JOURNAL OF SOLID STATE CHEMISTRY
www.elsevier.com/locate/jssc

# Kinetics study on phase transformation from titania polymorph brookite to rutile

Jason Huberty, Huifang Xu*

*Department of Geology and Geophysics, Materials Science Program, University of Wisconsin-Madison, 1215 West Dayton Street, Madison, WI 53706, USA*

Received 21 October 2007; received in revised form 14 December 2007; accepted 19 December 2007
Available online 25 December 2007

**Abstract**

$TiO_2$ is a polymorphic material of great scientific interest due to its semiconductor properties and uses in heterogeneous photocatalysis. Understanding the stability of the polymorphs is important for designing $TiO_2$-based photocatalysts and solar cells. Although the phase transformation of anatase → rutile has been well studied, there is only one published work on brookite → rutile to date. The brookite → rutile transformation has been studied in this work using natural material from the Magnet Cove igneous complex mechanically processed to several micrometers in size. The pure phase brookite is annealed from 800 to 900 °C without detection of the anatase polymorph. The transformation kinetics are described by both the standard first-order model, with an activation energy of $E_a = 411.91$ kJ/mol, and the Johnson–Mehl–Avrami–Kolmogorov (JMAK) model, with an activation energy of $E_a = 492.13$ kJ/mol. The rate parameter of the first-order model for the phase transformation is expressed as $k = 6.85 \times 10^{14} \exp(-49{,}451/T)\,s^{-1}$ for the first-order model and $k = 4.19 \times 10^{18} \exp(-59{,}189/T)\,s^{-1}$ using the JMAK model. The obtained activation energy is higher than that of brookite nano-crystals. Our results show that the JMAK model fits the kinetics data better than other models.


*Keywords:* Phase transition kinetics; XRD; Brookite; Rutile; Oxide semiconductor; Niobium doping; Rietveld analysis

## 1. Introduction

Crystals of $TiO_2$ polymorphs are oxide semiconductors that are both physically and chemically stable. The $TiO_2$ crystals can be used as heterogeneous photocatalysts that can use light energy to drive reactions like photocatalytic production of hydrogen from water and oxidation of organic compounds in air and water [1–5]. $TiO_2$ micro-crystals and nano-crystals are also used in dye-sensitized solar cells [1,6–8]. Because rutile is the most thermodynamically stable polymorph, it is necessary to understand the kinetics of phase transformations from other polymorphs into rutile. In nature, $TiO_2$ occurs as a common accessory mineral in igneous and metamorphic rocks and beach sands. The four polymorphs of $TiO_2$ that are stable on Earth are rutile (tetragonal), anatase (tetragonal), brookite (orthorhombic) and the high-pressure phase $TiO_2$ (II) with $\alpha$-type $PbO_2$ structure [9]. Brookite is formed by zig-zag chains of octahedra that share four edges. Rutile is formed by zig-zag chains of octahedra that share two edges. Viewed on (010), the brookite octahedra alternately point toward positive or negative *c*-axis. Rutile is formed by edge sharing octahedra along [001] with corner sharing along [110] and [1$\bar{1}$0]. The octahedral chains are rotated at 90° in rutile and nearly 90° in brookite but are not rotated to a large degree in the anatase structure. Rutile is the most thermodynamically stable form while anatase and brookite are metastable and are thought to occur at low temperatures and pressures. The phase stability field of brookite remains undefined. Phase transformation of anatase and brookite to rutile is reconstructive and proceeds directly without involvement of the other metastable phase. The anatase → rutile phase transformation has been studied by numerous investigators [10–13]. Zhang and Banfield [14] have summarized the previous work on anatase-to-rutile kinetics and proposed a modified kinetics model that considers size dependence and interface nucleation factors

*Corresponding author. Fax: +1 608 262 0693.
*E-mail address:* hfxu@geology.wisc.edu (H. Xu).

0022-4596/$ - see front matter © 2008 Published by Elsevier Inc.
doi:10.1016/j.jssc.2007.12.015

on the reaction rate. To date, only one study of brookite→rutile has been published and used monodispersed synthetic nano-crystals [15].

This study uses pure phase natural material obtained from Magnet Cove, Arkansas. The Magnet Cove Igneous Complex is a 94 million years old (Ma) [16] calc-alkaline igneous intrusion into folded Paleozoic sedimentary rocks. Erickson and Blade [20] describe the general geology and interpret the ring-like structure and complex igneous bodies as the eroded roots of a collapsed caldera. The mid-Cretaceous igneous activity in Arkansas follows a southeast to northeast trend possibly caused by the passage of North America over the Bermuda hotspot [16,17]. Fluids derived from late-stage carbonatites-carried titanium, niobium and molybdenum which mineralized the country rocks [18,19]. The titanium was complexed as $K_2TiF_6H_2O$ or $Na_2TiF_6H_2O$ and transported as a vapor phase derived from carbonatite magmas [18]. Apatite occurs in the igneous complex as the dominant F mineral phase. Rutile mineralization is associated with taeniolite which contains up to 8% F. Brookite mineralization occurred later without fluorine mineral phases [18]. The titanium in final stage fluids formed brookite on quartz aggregates within the folded and fractured novaculite [19]. Veins of brookite-quartz aggregates occur in the lower division of the novaculite, the source of the recrystallized silica. The clay mineralization occurred in altered shale seams in the novaculite [18,20].

Three main economic areas are defined in the complex: the Magnet Cove Co. rutile deposit, the Hardy–Walsh prospect and the Christy deposit. The latter two are both located in the folded layers of Arkansas novaculite. The Christy deposit is located on the east side of Magnet Cove one mile south of the Hardy–Walsh. Brookite occurs within quartz-brookite aggregate vein material and in remineralized novaculite.

## 2. Experimental method

The brookite for this work was obtained from a specimen of Magnet Cove material. The specimen displays euhedral brookite and quartz crystals in red clay. Brookite occurs as orthorhombic dipyramids from 2 to 10 mm in size with vicinal planes on {100} and well developed {112} (Fig. 1). Several 2–3 mm crystals were removed, cleaned and then mechanically processed to a powder with an average size of several micrometers. The source of our sample was likely vein material within the novaculite from the Christy deposit or one of the Hwy 270 outcrops known to produce large brookite crystals [18]. The average composition of the brookite is ($Ti_{0.966}$, $Nb_{0.016}$, $Fe_{0.01}$, $V_{0.008}$) $O_2$ [19].

Natural brookite and rutile paramorph brookite material were verified as pure phases using X-ray diffraction (XRD) (Fig. 2). X-ray characterization was done on a Scintag Pad V Diffractometer with Cu$K\alpha$ radiation. The samples were prepared as a film on a low background

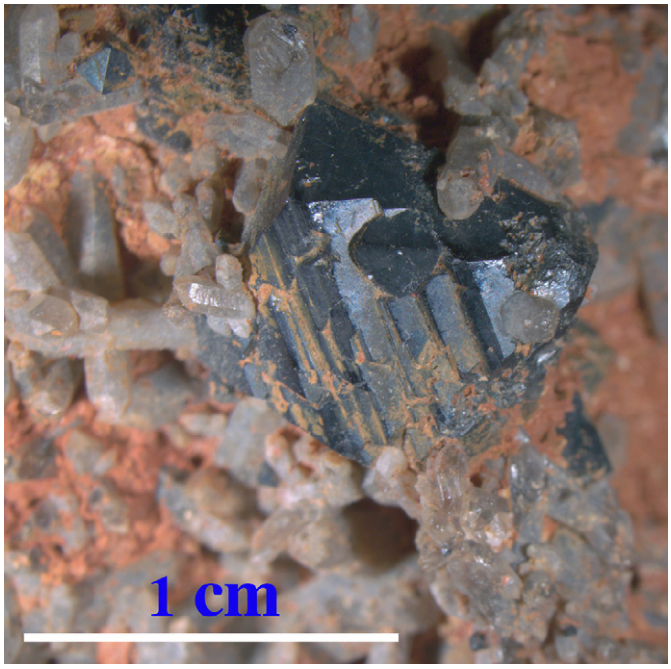


Fig. 1. Photo showing euhedral black brookite crystals and associated minerals of white quartz and red clays.

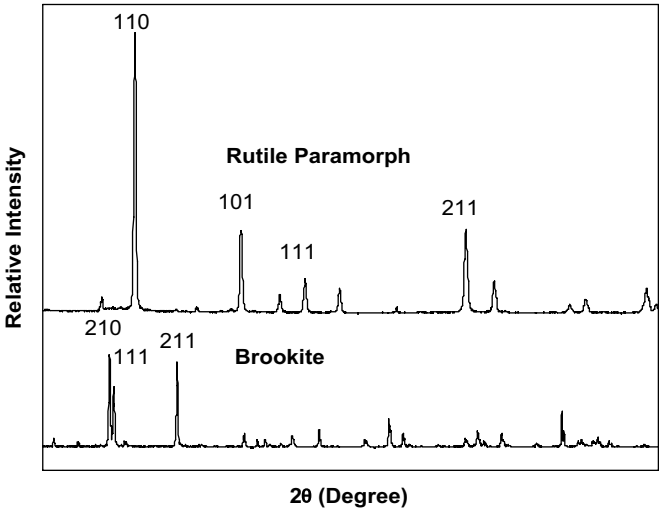


Fig. 2. Diffraction data for pure phase brookite and rutile paramorph specimens from Magnet Cove, AR.

quartz sample holder used to obtain higher-quality patterns. Scan parameters used are $2\theta$ angle 20–70°, step size 0.02° and dwelling time of 2 s. Samples consisting of 0.05 g brookite were annealed between 800 and 900 °C up to 40 h. XRD patterns obtained from annealed samples were used for the calculation of weight fraction of the two phases (Figs. 3–5).

Rietveld refinement method was then used to determine the weight fraction of rutile and brookite in the annealed samples. The Rietveld method uses a least-squares approach to refine a theoretical line profile until it matches the experimental profile obtained by standard powder

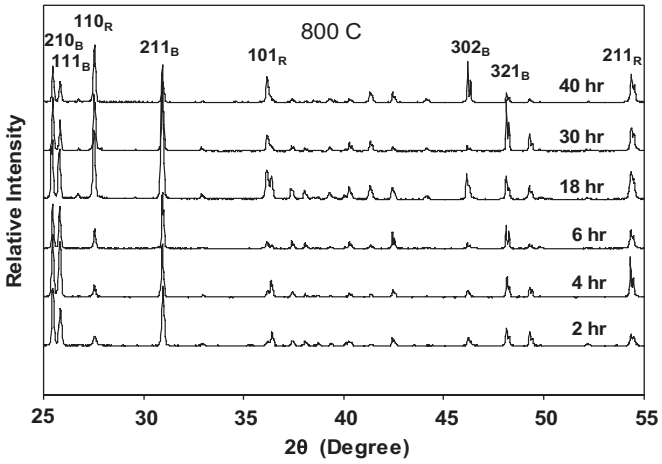


Fig. 3. Diffraction data for annealed samples at 800 °C.

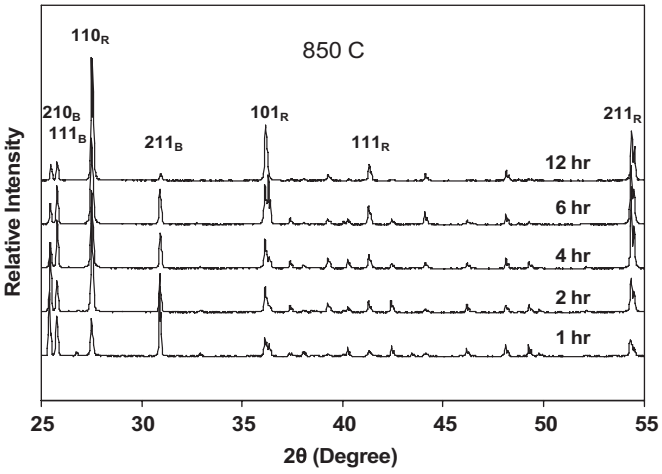


Fig. 4. Diffraction data for annealed samples at 850 °C.

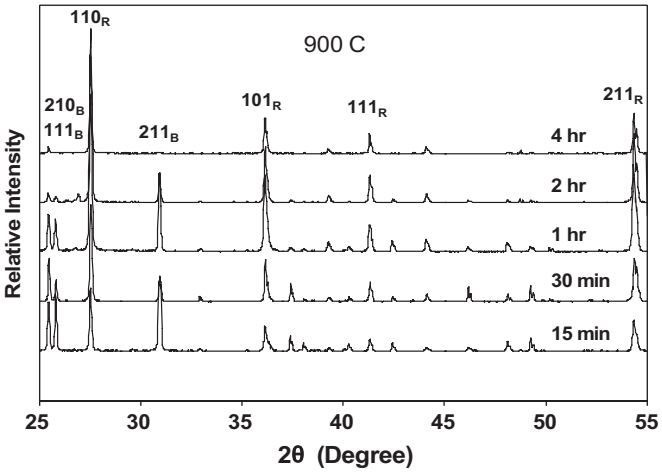


Fig. 5. Diffraction data for annealed samples at 900 °C.

XRD. The Rietveld method was used to refine the crystal structure of the phase and quantifies weight percentages of brookite and rutile phases. General structure analysis software (GSAS) [21] was used with EXPGUI, a free Windows structure refinement software [22]. Rietveld refinement allows for a more precise determination of phase weight fraction than traditional full-width at half-maximum calculations and corrects for preferred orientation.

Transmission electron microscopy (TEM) of the brookite and transformed rutile at 900 °C was done using a Philips CM 200UT microscope with a spherical aberration coefficient ($C_s$) of 0.5 mm and a point-to-point resolution of 0.19 nm. The TEM samples were prepared by depositing the powder samples on holey carbon-coated Cu grids.

## 3. Results and discussion

### 3.1. Phase transformation sequence

Phase transformation from brookite-to-rutile was observed without the presence of anatase as an intermediate phase. Standard X-ray powder diffraction technique was used to analyze each annealed sample. Several patterns were obtained to reduce the preferred orientation observed during phase transformation. Quartz (0.1%) was variably detected in some samples and is likely from material in the original specimen that contaminated the sample during separation. The Rietveld refinement also included quartz as a phase if there is small amount of quartz impurity. Rutile and brookite fractions were normalized. Quartz is not present in large enough amount to affect the phase transformation.

Refined lattice parameters for brookite pure phase starting material were determined to be $a = 9.1858$ ($\pm 0.0015$), $b = 5.4591$ ($\pm 0.0015$) and $c = 5.1430$ ($\pm 0.0015$) Å using the Rietveld technique yielding a density $\rho = 4.184\,g/cm^3$. These values are slightly larger than those from the data file ($a = 9.181580$, $b = 5.456076$ and $c = 5.139894$ Å) [23]. Rutile paramorph brookite material from Magnet Cove was identified as phase pure rutile using XRD (Fig. 2). Refined lattice parameters for rutile paramorph were determined to be $a = 4.5985$ ($\pm 0.0015$) and $c = 2.9637(\pm 0.0015)$ Å yielding a density $\rho = 4.201\,g/cm^3$. These values are also slightly larger than the ones given in the data file ($a = 4.5937$, $c = 2.9581$ Å) 23. The presence of Nb, V and Fe in the Ti octahedral site are likely the reason for enlarged cell parameters [19].

The brookite from brookite-quartz aggregates in the Christy deposit has been shown to contain 2% Nb, and 0.1% Fe and V [19]. Rietveld refinement of pure phase brookite improves with adjusting the Ti occupancy to include Nb, V and Fe at average values for brookite.

XRD patterns of annealed brookite at temperatures of 800, 850 and 900 °C are displayed in Figs. 3–5. A typical pattern of Rietveld analysis for obtaining amount of rutile is illustrated in Fig. 6. The weight fraction of rutile ($\alpha$) transformed at various temperatures is shown as a function of time (Fig. 7). The phase transformation occurred with 96% rutile produced in 4 h at 900 °C. With 40 h of

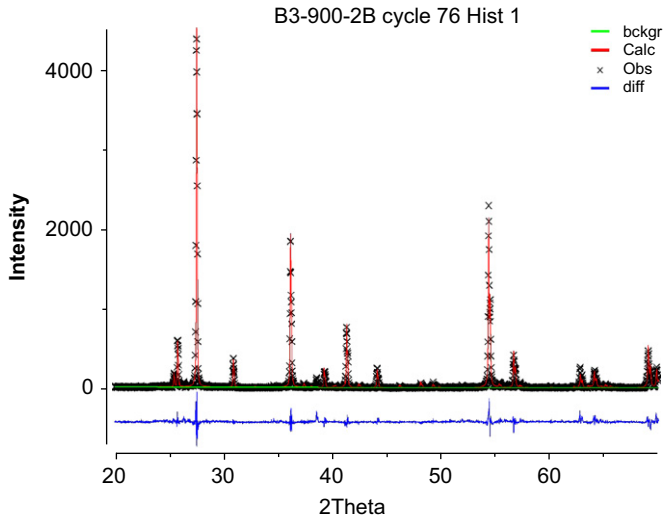


Fig. 6. A typical Rietveld refinement result of annealed brookite at 900 °C for 2 h.

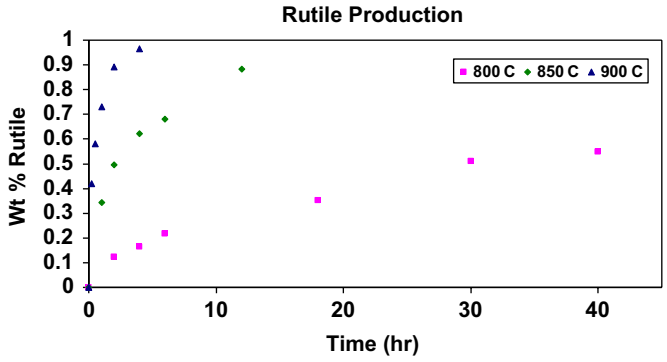


Fig. 7. Weight fraction of rutile as a function of time.

annealing at 800 °C, 55% rutile was produced (Fig. 7). No anatase was detected as an intermediate phase in any of the samples based on the diffraction patterns in agreement with previous work [15].

The Rietveld technique corrects for preferred orientation in the diffraction patterns. The preferred orientation of the same reflections in both phases suggests that the phase transformation may take place with the formation of regular and smooth surfaces through re-organization of the crushed grains at high temperatures. The phenomenon is obvious for the small submicron size grains (Fig. 8). Some transformed rutile may be paramorphs of the brookite, similar to the paramorph morphology observed in natural rutile paramorph after brookite macroscopic crystals from Magnet Cove. Further TEM work is needed to explain these observations.

No niobium-rich phase precipitates were observed in the transformed rutile, which suggests that niobium in the brookite structure is preserved in the transformed rutile. Niobium has been shown to hinder the phase transition for anatase to rutile and may affect the brookite-to-rutile transition similarly. Previous work on anatase to rutile

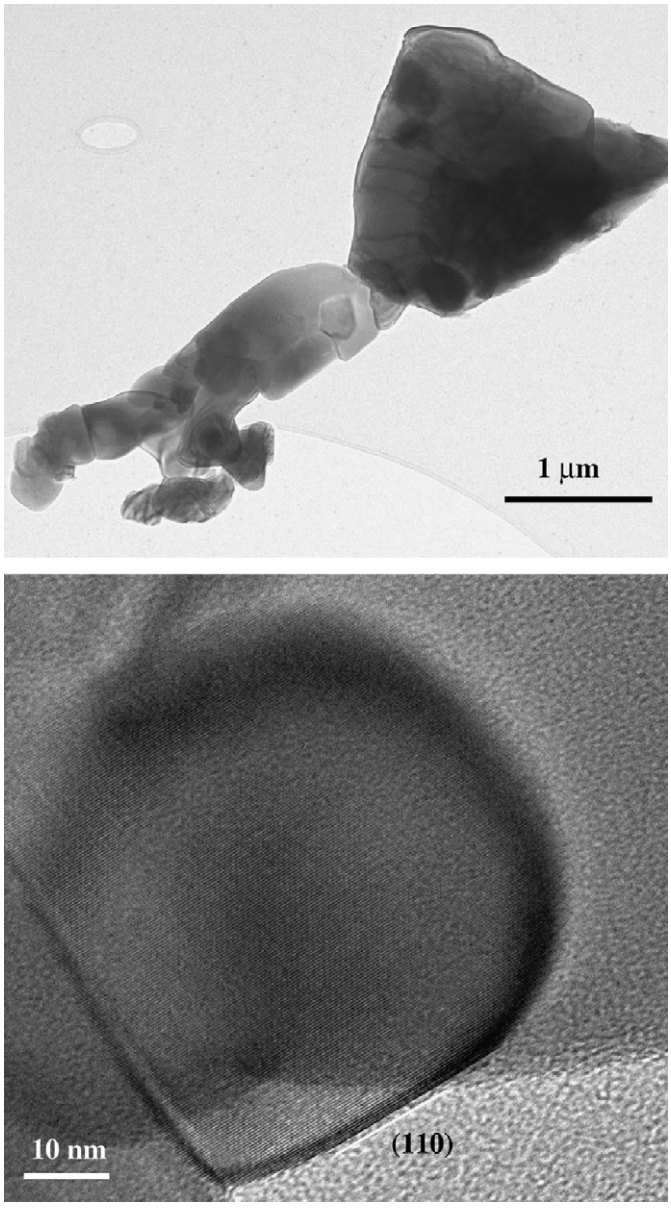


Fig. 8. Bright-field TEM image and high-resolution TEM image showing sintering of rutile crystals transformed from brookite at 900 °C (upper), and well developed (110) surface of a small crystal (lower).

shows that Nb is removed from the anatase prior to phase transformation and forms a thin film or cluster of Nb-oxide precipitates [24]. It is suggested that the resulting vacancies in anatase facilitate the phase transition [24]. We did not observe formation of Nb film or precipitates in our samples. The charge balance in brookite is maintained by the addition of vanadium and ferric iron, which may also affect the phase transformation although we did not observe this.

### 3.2. Phase transformation kinetics

Various kinetics models, summarized in Table 1, were employed to describe the kinetics of the phase

Table 1

| Kinetics models references | Equation |
|---|---|
| 1. Standard first order [32,28,33] | $\ln(1-\alpha) = -kt$ |
| 2. Standard second order [34] | $(1-\alpha)^{-1} - 1 = kt$ |
| 3. Contracting spherical interface [35–37] | $(1-\alpha)^{1/3} = kt + c$ |
| 4. Nucleation and growth of overlapping nuclei [36,37] | $[-\ln(1-\alpha)]^{1/3} = kt$ |
| 5. One dimensional, linear, branching nuclei and constant growth [36,37] | $\ln \alpha = kt + c$ |
| 6. Random nucleation and rapid growth [36,37] | $\ln(1-\alpha) = kt + c$ |
| 7. Johnson–Mehl–Avrami–Kolmogorov (JMAK) model [11,38,39] | $\ln -[\ln\ (1-\alpha)] = n \ln k + n \ln t$ |

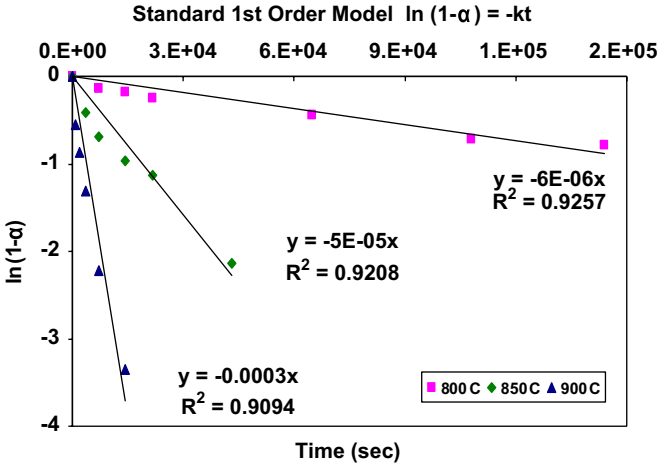


Fig. 9. First-order kinetics plot of transformation data.

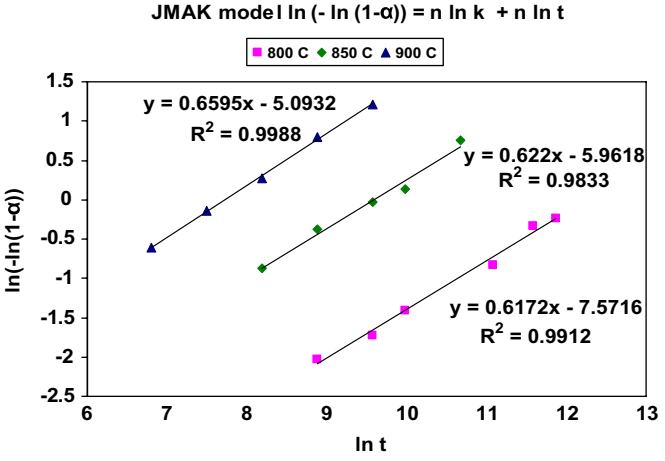


Fig. 10. JMAK plot of transformation data.

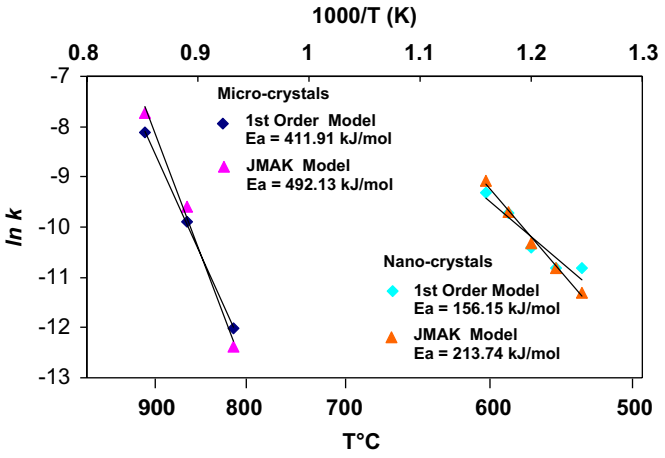


Fig. 11. Arrhenius plot of this work compared with same kinetics models using data from Li and Ishigaki [15].

transformation. Of the selected models, the standard first-order kinetics model and the Johnson–Mehl–Avrami–Kolmogorov (JMAK) model best fit the obtained data.

First-order rate laws describe the change in reaction rate for a single reactant in the system. Integrated rate laws describe the change in the rate over time. For first-order integrated rate laws, a plot of $\alpha$-$\ln(t)$ produces a straight line. The rate, $k$, can be obtained from the slope and then plotted against $1/T$ to obtain the activation energy via Arrhenius law. Straight lines were obtained using first-order kinetics models for our data (Fig. 9). Deviations for short annealing temperatures exist. An Arrhenius plot of $\ln k - 1/T$ yields a straight line with a slope of $-E_a/R$ (Fig. 11). The first-order kinetics model results in a rate parameter, $k = 6.85 \times 10^{14} \exp(-49{,}451/T)\,s^{-1}$ and an activation energy, $E_a = 412$ kJ/mol.

The widely used JMAK model is useful for describing first-order reconstructive polymorphic phase transformations [25,26]. A rate equation with a sigmoidal curve in a $\alpha - t$ plot is referred to as an Avrami equation. A reaction conforming to JMAK model gives a straight line when $\ln[-\ln(1-\alpha)]$ is plotted against annealing time, $t$. Straight lines were obtained using the JMAK model for our data (Fig. 10). The results fit the JMAK model well. Limitations on the JMAK equation as described for very fine nanometer size material are not applicable [14,27]. Phase transformation of nano-crystalline particles involves interface nucleation and constant nuclei growth modifications to the JMAK model [14].

The Avrami exponent, $n$, describes the reaction mechanism and is derived from the slope [28]. The exponent is expressed as an integer between 1 and 4 for polymorphic transformations. When $n = 1$, the JMAK model describes first-order kinetics [28]. Avrami exponent values of $n = 0.62$–$0.66$ were obtained from the JMAK plot of the obtained data (Fig. 11). The exponent value is nearly 2/3, which fits the model of growth along dislocations (Table 2) [25,29]. Kumar [11,12] also suggests transformation along dislocations and vacancies to explain the $n$ value of 0.66 obtained in their study. The obtained value of $n$ approximates the first-order model when $n = 1$. The JMAK model results in a rate parameter, $k = 4.19 \times 10^{18} \exp(-59189/T)\,s^{-1}$ and an activation energy, $E_a = 492$

Table 2
Values of exponent $n$ for JMAK equation modified from Burke 1992

| | $N$ |
|---|---|
| (a) Diffusion-controlled growth of a fixed number of particles | 3/2 |
| (b) Growth of a fixed number of particles limited by the interface process | 3 |
| (c) Diffusion-controlled growth of cylinders in axial direction only | 1 |
| (d) Diffusion-controlled growth of discs of constant thickness | 2 |
| (e) Growth on dislocations | 2/3 |
| (f) Nucleation at a constant rate and diffusion-controlled growth | 5/2 |
| (g) Growth of a fixed number of eutectoid cells | 3 |
| (h) Nucleation at a constant rate and growth of a eutectoid | 4 |

kJ/mol (Fig. 11). For comparison purpose, we also plotted the data from nano-brookite together with our data based on the same kinetics models (Fig. 11). The difference in their slopes indicates lower activation energy for the phase transformation from brookite nano-crystals to rutile than that from the micron size brookite crystals.

The previous work of Li and Ishigaki [15] using the JMAK model demonstrated non-linearity due to finite size limitations of the monodispersed nano-particles. An Avrami exponent of $n = 0.7$–$1.4$ was obtained for Li and Ishigaki's data. Previous works for the anatase→rutile phase transformation used the JMAK model successfully. Suzuki [38] obtained $n = 0.34$–$1.61$ and $E_a = 439$–$448$ kJ/mol using synthesized anatase 0.2–0.7 μm in size for the anatase to rutile transformation experiments. The activation energy is close to the value obtained in this study for similar sized micron to sub-micron particles suggesting a similar mechanism and energy barrier for anatase→rutile and brookite→rutile. Kumar et al. [11,12] obtained $n = 0.66$ and $E_a = 147$ kJ/mol using synthesized anatase particles 6 nm size. The $n$ value is identical to the value obtained in this study and the activation energy is close to that obtained for nano-particles of brookite by Li and Ishigaki [15]. The similar $n$ values (0.66) and activation energies at bulk and nano-size for anatase→rutile and brookite→rutile are not surprising considering both are polymorphic first-order reconstructive phase transformations. It can be inferred that the energies required to break bonds in both anatase and brookite should be similar.

There is a known surface energy effect on phase transformation for anatase to rutile. With decreasing particle size, surface energies contribute more to the Gibbs free energy of formation [30]. The stabilities of rutile and anatase switch below 14 nm [13,31]. It is unknown if brookite stability is similarly affected for nano-size material. The thermodynamic contribution of surface energy for a given particle size is much lower for bulk materials than nano-sized crystals.

## 4. Conclusions

The brookite→rutile phase transformation has been studied using natural pure phase material from Magnet Cove igneous complex mechanically processed to micron size grains. The phase transition experiments were carried out in the temperature range of 800–900 °C and the brookite transforms directly to rutile without detection of anatase as an intermediate phase. The reaction rate is best expressed by standard first-order kinetics and the JMAK model with an Avrami exponent value of $n = 0.62$–$0.66$ that indicates growth along defect sites like dislocations and vacancies. The first-order model results in a rate parameter, $k = 6.85 \times 10^{14} \exp(-49{,}451/T)\,s^{-1}$ and an activation energy, $E_a = 412$ kJ/mol. The JMAK model results in a rate parameter, $k = 4.19 \times 10^{18} \exp(-59{,}189/T)\,s^{-1}$ and an activation energy, $E_a = 492$ kJ/mol. Future works to determine size dependence in brookite→rutile phase transformation are necessary.

## Acknowledgments

We thank three anonymous reviewers for constructive comments. This research is supported by the Department of Geology and Geophysics, the University of Wisconsin-Madison, and NASA Astrobiology Institute.

## References

[1] A. Fujishima, K. Honda, Nature 238 (5358) (1972) 37.
[2] A. Fujishima, K. Hashimoto, H. Watanabe, 1997, BKC Inc., Tokyo.
[3] H. Xu, G. Vanamu, Z. Nie, H. Konishi, R.R. Yeredla, J. Phillips, Y. Wang, J. Nanomater. 2006 (2006) Article ID 78902, 1–8.
[4] R.R. Yeredla, H. Xu, Nanotechnology 19 (2008) 055706 (10pp).
[5] R.R. Yeredla, H. Xu, J. Phys. Chem. C 23 (2008) in press.
[6] B. Oregan, M. Gratzel, Nature 353 (6346) (1991) 737–740.
[7] K. Tanaka, M.F.V. Capule, T. Hisanaga, Chem. Phys. Lett. 187 (1–2) (1991) 73–76.
[8] J.M. Herrmann, C. Guillard, J. Disdier, C. Lehaut, S. Malato, J. Blanco, Appl. Catal. B—Environ. 35 (4) (2002) 281–294.
[9] J.F. Banfield, D.R. Veblen, Am. Mineral. 77 (1992) 545–557.
[10] A. Suzuki, T. Ritushi, Bull. Chem. Soc. Jpn. 42 (1969) 1853–1857.
[11] K.N.P. Kumar, K. Keizer, A.J. Burggraaf, J. Mater. Chem. 3 (1993) 1141–1149.
[12] K.N.P. Kumar, K. Keizer, A.J. Burggraaf, T. Okubo, H. Nagamoto, J. Mater. Chem. 3 (1993) 1151–1159.
[13] A.A. Gribb, J.F. Banfield, Am. Mineral. 82 (1997) 717–728.
[14] H. Zhang, J.F. Banfield, Am. Mineral. 84 (1999) 528–535.
[15] J.-G. Li, T. Ishigaki, Acta Mater. 52 (2004) 5143–5150.
[16] A. Baksi, J. Geol. 105 (1997) 629–643.
[17] W.J. Morgan, Tectonophysics 94 (1983) 327–348.
[18] V.C.J. Fryklund, D.F. Holbrook, Div. Geol. (1950) bulletin 16.
[19] M. Flohr, Econ. Geol. 89 (1994) 105–130.
[20] R.L. Erickson, L.V. Blade, US Geological Survey Professional Paper 425, 1963.
[21] A.C. Larson, R.B.V. Dreele, Los Alamos National Laboratory Report, 2000.
[22] B.H. Toby, J. Appl. Crystallogr. 34 (2001) 210–213.
[23] R.W.G. Wyckoff, Crystal Structures. 2nd ed., vol. 1, Wiley, New York, 1963, pp. 250–255.
[24] J. Arbiol, J. Cerda, G. Dezanneau, A. Cirera, F. Peiro, A. Comet, J.R. Morante, J. Appl. Phys. 92 (2) (2002) 853–861.

[25] R.J. Borg, G.J. Dienes, The Physical Chemistry of Solids, Academic Press, San Diego, CA, 1992, 525pp.
[26] A. Putnis, Introduction to Mineral Sciences, Cambridge University Press, UK, 1992, pp. 315–318.
[27] M.C. Weinberg, D.P. Birnie III, V.A. Shneidman, J. Non-Cryst. Solids 219 (1997) 89–99.
[28] C.N.R. Rao, K.J. Rao, Phase Transitions in Solids, 1978, pp. 91–95.
[29] J.E. Burke, Progress in Ceramic Science, vol. 1, Pergamon Press, New York, 1960, p. 1.
[30] A.S. Barnard, P. Zapol, J. Phys. Chem. B 108 (2004) 18435–18440.
[31] H.Z. Zhang, J.F. Banfield, J. Mater. Chem. 8 (9) (1998) 2073–2076.
[32] A. Suzuki, Y. Kotera, Bull. Chem. Soc. Jpn. 35 (1962) 1353–1357.
[33] J.F. Banfield, B.L. Bischoff, M.A. Anderson, Chem. Geol. 110 (1993) 211–231.
[34] A.W. Czanderna, C.N.R. Rao, J.M. Honig, Trans. Faraday Soc. 54 (1958) 1069–1073.
[35] E.F. Heald, C.W. Weiss, Am. Mineral. 57 (1972) 10–23.
[36] K.J.D. MacKenzie, Trans. J. Br. Ceram. Soc. 74 (1975) 77–84.
[37] R.D. Shannon, J.A. Pask, Am. Mineral. 49 (1964) 1707–1717.
[38] A. Suzuki, R. Tukuda, Bull. Chem. Soc. Jpn. 42 (1969) 1853–1857.
[39] S. Hishita, I. Mutoh, K. Koumoto, H. TYanagida, Ceram. Int. 9 (1983) 41–47.